# Unimolecular dissociation dynamics of disilane

Paras M. Agrawal, Donald L. Thompson, and Lionel M. Raff

Citation: The Journal of Chemical Physics **92**, 1069 (1990); doi: 10.1063/1.458169
View online: http://dx.doi.org/10.1063/1.458169
View Table of Contents: http://scitation.aip.org/content/aip/journal/jcp/92/2?ver=pdfcov
Published by the AIP Publishing

# Unimolecular dissociation dynamics of disilane

Paras M. Agrawal, Donald L. Thompson, and Lionel M. Raff
*Department of Chemistry, Oklahoma State University, Stillwater, Oklahoma 74078*

(Received 30 June 1989; accepted 5 October 1989)

The unimolecular dissociation dynamics of disilane are investigated using classical trajectory methods with a global potential-energy surface fitted to the available experimental data and the results of various *ab initio* calculations. The potential surface is written as the sum of 52 many-body terms containing 86 adjustable parameters which are fitted to experimental and/or calculated data for stationary point geometries, fundamental vibrational frequencies, reaction endo- and exothermicities, and potential-energy barrier heights for reactions of disilane and molecules derived from disilane. In general, the equilibrium bond lengths and angles for $Si_2H_6$, $Si_2H_5$, $H_3Si$–$SiH$, $H_2Si=SiH_2$, $H_2Si=SiH$, $H_2Si=Si$, $HSi=Si$, $Si_2$, $H_2$, and $SiH_2$ given by the global potential agree with *ab initio* results to within 0.03 A and 2°, respectively, or better. The predicted heats of reaction for 13 reactions involving disilane or its derivatives are in good accord with the experimental and *ab initio* results. The average absolute deviation is 3.55 kcal/mol. The average absolute difference between the normal-mode frequencies given by the global potential for $Si_2H_6$, $Si_2H_5$, and $H_3Si$–$SiH$ and those obtained from scaled MP4 calculations are 58.7, 52.1, and 62.8 $cm^{-1}$, respectively. If two low-frequency Si–Si–H deformation modes for each of these molecules are omitted from consideration, the average absolute differences are all in the range 34–36 $cm^{-1}$. The calculated barrier height for the hydrogen-atom transfer process leading to $SiH_4 + SiH_2$ products is 56.7 kcal/mol. For three- and four-center $H_2$ elimination reactions, the barrier heights given by the global surface are 60.1 and 91.1 kcal/mol, respectively. These values are all within 1.2 kcal/mol of the results obtained by Ho *et al.* from MP4 calculations. The $Si_2H_6$ dissociation dynamics at seven internal energies ranging from 5.31 to 9.31 eV have been investigated. At low internal energy, dissociation leading to $SiH_4 + SiH_2$ dominates the dynamics. At internal energies in the range $5.31 \leqslant E \leqslant 6.31$ eV, the various $Si_2H_6$ decomposition channels are, in order of importance, hydrogen-atom transfer leading to $SiH_4 + SiH_2$, Si–Si bond rupture giving two $SiH_3$ radicals, three-center $H_2$ elimination, Si–H bond rupture to give $Si_2H_5 + H$, and four-center $H_2$ elimination to give $H_2Si=SiH_2$. At higher internal energies, entropy effects cause an inversion of this ordering such that Si–Si bond rupture becomes the major decomposition channel followed by three-center $H_2$ elimination, $SiH_4 + SiH_2$ formation, Si–H bond rupture, and four-center $H_2$ elimination. The present results suggest that the formation of disilene in disilane pyrrolysis occurs predominantly via the formation of $H_3Si$–$SiH$ from three-center $H_2$ elimination followed by a low-barrier hydrogen transfer process. For all decomposition channels, most of the available energy is partitioned in vibrational modes of the products. To a large extent, product energy partitioning is found to be governed by statistical considerations. Exceptions to this generalization are found in three-center $H_2$ elimination and for any product which involves the formation of a new bond. We find that while three-center $H_2$ elimination is a concerted reaction, it probably does not occur along a symmetric pathway. Hydrogen transfer to form $SiH_4 + SiH_2$ is found to be a concerted process, but four-center $H_2$ elimination involves the rupture of one Si–H bond followed by hydrogen transfer and a subsequent $H_2$ abstraction reaction to give the $H_2 + H_2Si=SiH_2$ products.

## I. INTRODUCTION

The chemical vapor deposition of silicon from silane[1,2] involves a large number of heterogeneous and homogeneous reactions.[1–5] The primary product of the dissociation of silane is $SiH_2$. Once formed, $SiH_2$ can undergo further decomposition to form silicon atoms and $H_2$[5] or it can condense with $SiH_4$ to form disilane

$$SiH_4 + SiH_2 \rightarrow Si_2H_6^*, \quad \text{(R1)}$$

where the superscript * denotes a vibrationally excited molecule. The $Si_2H_6^*$ molecules formed in reaction (R1) subsequently undergo unimolecular decomposition into a variety of channels that include

$$Si_2H_6^* \rightarrow SiH_4 + SiH_2, \quad \text{(R2)}$$

$$Si_2H_6^* \rightarrow SiH_3 + SiH_3, \quad \text{(R3)}$$

$$Si_2H_6^* \rightarrow H_3Si\text{–}SiH + H_2, \quad \text{(R4)}$$

$$Si_2H_6^* \rightarrow H_3Si\text{–}SiH_2 + H, \quad \text{(R5)}$$

and

$$Si_2H_6^* \rightarrow H_2Si=SiH_2 + H_2. \quad \text{(R6)}$$

The products formed in reactions (R2)–(R6) may undergo further dissociation which ultimately leads to the formation

 0021-9606/90/021069-14$03.00  

of the $Si_2$ dimer. For example,

$$H_3Si\text{–}SiH \rightarrow HSi = SiH + H_2 \quad \text{(R7)}$$

followed by

$$HSi = SiH \rightarrow Si_2 + H_2. \quad \text{(R8)}$$

We have previously reported theoretical studies of the unimolecular decomposition reactions of disilene,[5] which can be formed via reactions such as (R6).

The modeling studies reported by Coltrin *et al.*[6] suggest that the $Si_2$ dimer makes a significant contribution to the total silicon chemical vapor deposition (CVD) rate provided the temperature is in excess of 1150 K and the carrier gas is helium. Ho and Breiland[7] have also observed $Si_2$ in silicon CVD experiments using laser excited fluorescence. The elementary steps leading to the formation of $Si_2$, however, are unknown. The mechanism could involve termolecular recombination

$$Si + Si + M \rightarrow Si_2 + M, \quad \text{(R9)}$$

where M is any third body. However, the calculated rates for reaction (R9) when M is an argon atom,[8] combined with the low concentration of silicon atoms present in typical CVD experiments, suggests that reaction (R9) is not the major pathway leading to silicon dimer formation. More recent calculations for the case where M is a third silicon atom support this view.[9]

Coltrin *et al.*[6] have suggested that the reaction sequence (R1)–(R8) constitutes the major pathway for dimer formation. The high concentration of silane present in silicon CVD experiments plus the fact that $SiH_2$ is the primary dissociation product argue in favor of such a mechanism. A quantitative assessment, however, requires that the rate coefficients for each of these reactions be known. Our previous study of the $Si_2H_4$ decomposition dynamics[5] have provided much of the data required, but the rates for the dissociation of $Si_2H_6$ itself are still unknown.

The investigation of the decomposition dynamics of $Si_2H_6$ requires the formulation of an accurate global potential surface for the eight-body system. Since it is obviously impossible to carry out converged, multireferenced, complete configuration interaction (CI) calculations at a sufficiently large number of configuration points to completely characterize the multidimensional potential hypersurface for a system as complex as $Si_2H_6$, the problem can never be "solved." However, our experience has shown that this level of accuracy and completeness is not necessary to obtain useful results. If certain key elements of the potential surface are accurately described and if the choice of functional forms used to fit the available data is based on well-judged chemical and physical considerations, then the computed dynamics, rates, and mechanisms for the system are often in good to excellent accord with experiment, even though many of the finer details of the potential surface are incorrect.

In this paper, we report the development of an empirical global potential-energy surface for the $Si_2H_6$ system. We then obtain the dynamics and rates of reactions (R2)–(R6) from the results of trajectories computed on this surface. Subsequent sections of the paper describe the methods used to develop the potential surface and the trajectory results.

## II. $Si_2H_6$ POTENTIAL-ENERGY SURFACE

As discussed in the previous section, our aim is to develop a global representation of the $Si_2H_6$ potential-energy surface that will be useful in dynamics calculations of various types. Clearly, a brute force attempt to achieve this objective by computation of the energies of a large ensemble of configurations followed by least-square fitting to arbitrary functional forms is very unlikely to succeed. First, the number of points required to characterize the multidimensional surface is simply too large and second, arbitrarily chosen functional forms have the annoying feature of fitting well in one region of configuration space, but very poorly in others.

In principle, the total potential $V_T$ may be written as a many-body expansion of the form

$$V_T = \sum_i V_i, \quad (1)$$

where the $V_i$ are $i$-body terms and $V_T$ includes the sum of all possible such terms. Murrell and co-workers[10] have made effective use of such an expansion for systems in which $N < 4$. For more complex systems, however, the many-body expansion becomes computationally intractable. In fact, even for the case $N = 4$, it is extremely difficult to obtain surfaces that are sufficiently accurate in all important regions of configuration space. For the $Si_2H_6$ system with $N = 8$, it is essentially impossible.

Our approach is less ambitious. Rather than attempt to accurately describe all energetically accessible regions of the hypersurface, we focus upon the topographical features of the reactants, products, and the various transition states. In particular, we attempt to develop a surface which properly describes the fundamental vibration frequencies and geometries for reactants and products along with the thermochemistry for all open reaction channels. We also strive to represent the potential barriers for these channels accurately. Finally, we employ functional forms suggested by chemical and physical considerations. Such choices will often produce acceptable accuracy with regard to topographical features of the surface not directly addressed in the fitting process. We have previously applied this strategy in the development of potential hypersurfaces for $SiH_2$,[4,5] $Si_3$,[11] $Si_4$,[12] $Si_2H_4$,[4,5] and $FH_2C\text{–}CH_2F$.[13]

### A. Experimental and *ab initio* data

The available experimental data on the $Si_2H_6$ system includes the fundamental vibration frequencies and equilibrium geometries for disilane. Several kinetic measurements of the dissociation dynamics of disilane are also available. The experimental results reported by Purnell *et al.*[14] and by Ring *et al.*[15] show no evidence for the production of radicals in unimolecular dissociation reactions of $Si_2H_6$. Consequently, it may be inferred that the dissociation barrier for these products is very large. These experiments show that the major decomposition products are $SiH_4 + SiH_2$ and that the minor products are $H_2Si = SiH_2 + H_2$, which suggests a significantly larger barrier for the latter channel. However, Ring *et al.* have assumed that the barrier for direct formation of $H_2Si = SiH_2 + H_2$ is sufficiently low that reaction in this channel can be observed. Olbrich *et al.*[16] have

concluded that both $H_2Si=SiH_2$ and $H_3Si$–SiH are formed with activation energies of 52.1 and 55.7 kcal/mol, respectively.

Gordon *et al.*[17] and Ho *et al.*[18,19] have used electronic structure calculations to provide a wealth of information about the stationary points on the $Si_2H_6$ potential hypersurface as well as some additional information related to the potential barriers for various reaction channels. These calculations have been carried out at the MP4/6-31G** level at geometries determined in HF/6-31G* calculations. The data consist of equilibrium geometries, corrected harmonic vibrational frequencies (calculated at the HF/6-31G* level), and electron-correlated total energies for various $SiH_n$ ($n=1,2,3,4$) and $Si_2H_n$ ($n=1,2,\ldots,6$) species. In general, there is good agreement between the theoretical[17–19] and the experimental results.[14–16] The few points of disagreement that exist are discussed below.

### B. Functional form of the fitted surface

In this section, we develop an empirical $Si_2H_6$ potential-energy surface which represents most of the important open reaction channels for the system. Reaction channels leading to

$H_3Si$–$SiH_2 + H$,

$H_3Si$–$SiH + 2H$,

$H_3Si$–$SiH + H_2$,

$H_2Si=SiH_2 + 2H$,

$H_2Si=SiH_2 + H_2$,

$SiH_2 + SiH_4$,

$SiH_3 + SiH_3$,

$H_2Si$–$SiH + H + H_2$ or 3H,

$H_2Si$–$Si + 2H_2$ or $H_2 + 2H$ or 4H,

$Si_2 + 3H_2$ or other H combinations,

$HSi=Si + 2H_2 + H$ or other hydrogen combinations

are all open on the potential surface, although not all of these channels are described with equal accuracy.

The interparticle distances are defined as shown in Fig. 1. The angles are defined in Fig. 2. The portion of configuration space corresponding to $Si_2H_6$ and its reactions are represented by

$$V_{Si_2H_6} = V_{Si_2}(R_1) + \sum_{j=2}^{7} V_{SiH}(R_j) + \sum_{i=1}^{6} V_{H\text{-}Si\text{-}H}(\theta_i) + \sum_{i=7}^{12} V_{Si\text{-}Si\text{-}H}(\theta_i) + V^4_{HH} + V^3_{HH} + V_T. \quad (2)$$

The $V_{Si_2}$ term is the Si–Si bond potential. The $V_{SiH}$ terms are the six Si–H bond potentials. The $V_{H\text{-}Si\text{-}H}$ and $V_{Si\text{-}Si\text{-}H}$ terms are harmonic bending potentials for the H–Si–H and Si–Si–H angles, respectively. $V^4_{HH}$ and $V^3_{HH}$ are the terms that open the four-center and three-center $H_2$ dissociation pathways, respectively. The $V_T$ term governs the transfer of a hydrogen atom in the dissociation channel leading to $SiH_2 + SiH_4$.

The configuration space corresponding to disilene $H_2Si=SiH_2$ is represented by our previously formulated potential surface,[4,5] here denoted by $V_{Si_2H_4}$. The surface is combined with $V_{Si_2H_6}$ to form the complete hypersurface for the eight-atom system

$$V_{Total} = (1-S_1)V_{Si_2H_6} + S_1[V_{Si_2H_4} + V_{HH}], \quad (3)$$

where $S_1$ is a switching function.

The various terms in Eq. (3) have the following mathematical forms

#### 1. Si–Si term

$$V_{Si_2} = D_S\{\exp[-2A_S(R_1 - R_1^0)]\} - 2\exp[-A_S(R_1 - R_1^0)], \quad (4)$$

where

$$D_S = a(1) + [B - a(1)]\left(6 - \sum_{i=2}^{7} \exp\{-a(2) \times [R_i - a(10)]^2\}\right), \quad (5)$$

$$B = a(3) - a(4)\left(5 - \sum_{i=2}^{7} \exp\{-a(2)[R_i - a(10)]^2\}\right), \quad (6)$$

$$A_S = a(20) + [B' - a(20)]\left(6 - \sum_{i=2}^{7} \exp\{-a(2) \times [R_i - a(10)]^2\}\right), \quad (7)$$

$$B' = a(21) - a(22)\left(5 - \sum_{i=2}^{7} \exp\{-a(2) \times [R_i - a(10)]^2\}\right), \quad (8)$$

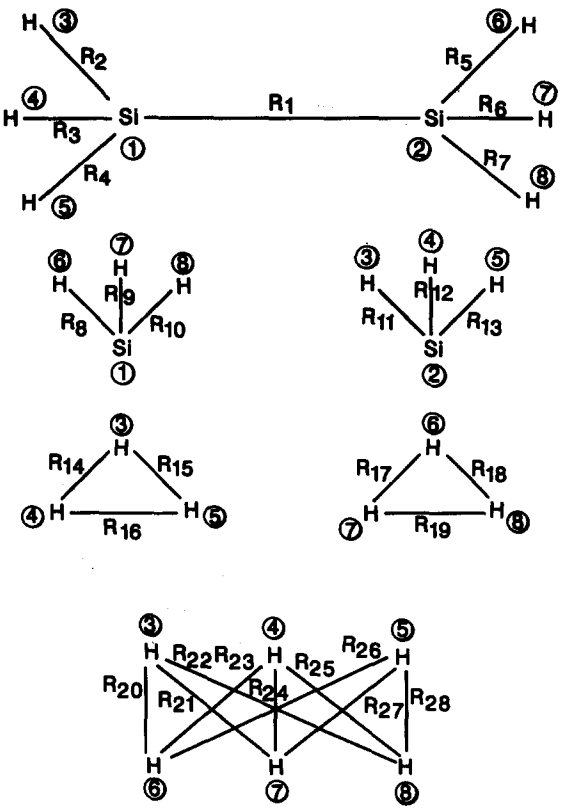


FIG. 1. Definitions of interatomic distances $R_i$ and atom numbers given within circles.

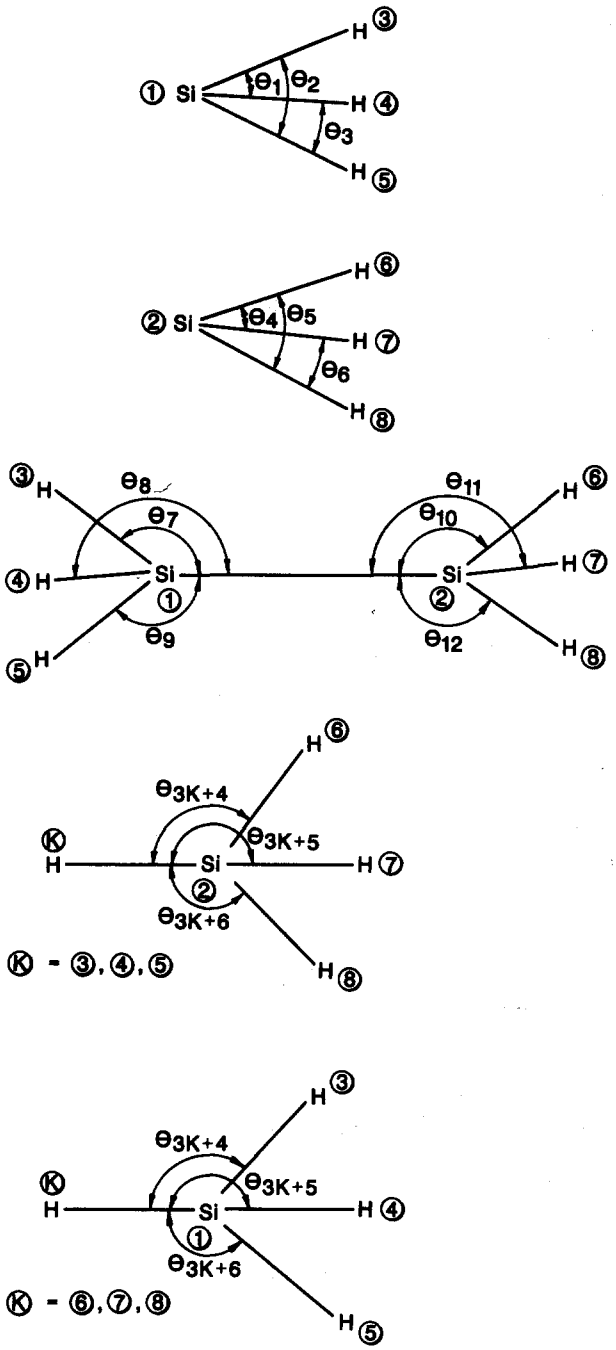


FIG. 2. Definitions of Si–Si–H and H–Si–H angles.

and

$$R_1^0 = a(11) + a(37)\exp\left[a(27)\left(2 - \sum_j \exp\{-a(16)\,[R_j - a(10)]^2\}\right)\right], \tag{9}$$

where the $j$ sum runs over the Si–H bond distances on the silicon atom with the fewer number of bonded hydrogen atoms and the $a(i)$ are adjustable parameters.

$V_{Si_2}$ describes the Si–Si interaction in terms of a modified Morse potential in which the "parameters" of the Morse function are themselves dependent upon the structure of the system. Equations (5) and (6) vary the Si–Si bond energy as the number of hydrogens atoms bonded to the silicon atoms vary. The limiting values are

$$\begin{aligned} D_S &= a(1) \quad \text{for } Si_2H_6, \\ &= a(3) \quad \text{for } Si_2H_5, \\ &= 2a(3) - 2a(4) - a(1) \quad \text{for } H_3Si\text{–}SiH. \end{aligned}$$

Equations (7) and (8) vary the Si–Si frequency parameter as the number of bonded hydrogen atoms changes. The limiting values are

$$\begin{aligned} A_S &= a(20) \quad \text{for } Si_2H_6, \\ &= a(21) \quad \text{for } Si_2H_5, \\ &= 2a(21) - 2a(22) - a(20) \quad \text{for } H_3Si\text{–}SiH. \end{aligned}$$

The equilibrium Si–Si bond length is determined by $R_1^0$. The limiting values of $R_1^0$ are

$R_1^0 = a(11) + a(37)\exp[-a(27)] \cong a(11)$, for disilane,

$R_1^0 = a(11) + a(37)$, for the disilyl radical $Si_2H_5$,

and

$R_1^0 = a(11) + a(37)\exp[a(27)]$, for $H_3Si$–SiH.

### 2. Si–H terms

$$V_{SiH}(R_i) = D_{SiH}(\exp\{-2C[R_i - a(10)]\} - 2\exp\{-C[R_i - a(10)]\})S_2S_3, \tag{10}$$

with

$$D_{SiH} = a(5) - a_6'\left(\sum_j \exp\{-a(9)\,[R_j - a(10)]^2\} - 4\right), \tag{11}$$

$$a_6' = a(6) + a_7'\left(\sum_j \exp\{-a(9)\,[R_j - a(10)]^2\} - 3\right), \tag{12}$$

$$a_7' = a(7) + a(8)\left(\sum_j \exp\{-a(9)\,[R_j - a(10)]^2\} - 2\right), \tag{13}$$

$$C = a(23) - b_6'\left(\sum_j \exp\{-a(9)\,[R_j - a(10)]^2\} - 4\right), \tag{14}$$

$$b_6' = a(24) + b_7'\left(\sum_j \exp\{-a(9)\,[R_j - a(10)]^2\} - 3\right), \tag{15}$$

$$b_7' = a(25) + a(26) \times\left(\sum_j \exp\{-a(9)\,[R_j - a(10)]^2\} - 2\right), \tag{16}$$

$$S_2 = \tanh\{a(42)\,[R_k - a(10)]\}, \tag{17}$$

and

$$S_3 = \prod_n (1.0 - \exp\{-a(19)\,[R_n - a(30)]^2\}), \tag{18}$$

where $R_k$ is the distance from the hydrogen atom to the second silicon atom. The product index $n$ runs over the five

possible H–H distances associated with the hydrogen atom forming the Si–H bond. Each of the above summations over $j$ run over the six distances between the silicon atom and the six hydrogen atoms.

Equation (10) describes the Si–H bond potential using modified Morse functions similar to Eq. (4). Equations (11)–(13) vary the Si–H bond energy for Si–H, $SiH_2$, $SiH_3$, and $SiH_4$ species. The limiting values are

$$D_{\mathrm{SiH}} = a(5) \quad \text{for } SiH_4,$$
$$= a(5) + a(6) \quad \text{for } SiH_3,$$
$$= 2a(6) - 2a(7) + a(5) \quad \text{for } SiH_2,$$

and

$$= a(5) + 3a(6) + 6a(8) - 6a(7) \quad \text{for SiH}.$$

Equations (14)–(16) modify the Si–H frequency parameter in a similar fashion. For $Si_2H_6$, the equilibrium Si–H bond distance is assumed to be a constant. For the portion of configuration space corresponding to $Si_2H_4$, however, the Si–H equilibrium bond length varies with the number of hydrogen atoms bonded to silicon.[4]

The Si–H bond interaction is attenuated by the $S_2$ switching function as a hydrogen atom is transferred to the second silicon atom in the reaction $Si_2H_6 \rightarrow SiH_2 + SiH_4$. The $S_3$ function attentuates the Si–H interaction as the hydrogen atom begins to form an H–H bond.

### 3. H–Si–H angle terms

$$V_{\mathrm{H\text{-}Si\text{-}H}}(\theta_i) = 0.5k_b[\theta_i - \theta_i^0]^2, \tag{19}$$

where

$$k_b = a(17)\exp(-a(12)\{[R_u - a(10)]^2 + [R_v - a(10)]^2\})], \tag{20}$$

with $R_u$ and $R_v$ being the two Si–H distances forming the H–Si–H angle. $\theta_i^0$ is taken to be constant and equal to $a(13)$.

### 4. Si–Si–H angle terms

$$V_{\mathrm{Si\text{-}Si\text{-}H}}(\theta_i) = 0.5k_b'[\theta_i - \theta_i^0]^2, \tag{21}$$

where

$$k_b' = a(18)\exp(-a(12)\{[R_1 - a(11)]^2 + [R_v - a(10)]^2\}) \tag{22}$$

with $R_v$ being the Si–H distance forming the Si–Si–H angle and

$$\theta_i^0 = a(14) + a(15)\exp\left[a(27)\left(2 - \sum_j \exp\{-a(16) \times [R_j - a(10)]^2\}\right)\right], \tag{23}$$

where the summation over $j$ runs over all Si–H bonds on the apex Si atom.

The H–Si–H and Si–Si–H bending terms are assumed to have a harmonic angle dependence with a force constant that attenuates in Gaussian fashion as the bonds forming the angle increase in length. The equilibrium H–Si–H angle is assumed to be constant, whereas Eq. (23) varies the equilibrium Si–Si–H angle as the number of Si–H bonds varies. The limiting values are

$$\theta_i^0 = a(14) + a(15)\exp[-a(27)] \quad \text{for } Si_2H_6,$$
$$= a(14) + a(15) \quad \text{for } Si_2H_5,$$
$$= a(14) + a(15)\exp[a(27)] \quad \text{for } H_3Si\text{–}SiH.$$

### 5. $V_{HH}^4$ term

The four-center $H_2$ dissociation terms have the form

$$V_{\mathrm{HH}}^4 = \sum_i V_{\mathrm{HH}}(R_i), \tag{24}$$

$$V_{\mathrm{HH}}(R_i) = a(28)(\exp\{-2a(29)[R_i - a(30)]\} - 2\exp\{-a(29)[R_i - a(30)]\}) \times A_2(R_u,R_v)A_4(R_k), \tag{25}$$

$$A_2(R_u,R_v) = (1 - \exp\{-a(31)[R_u - a(32)]^2\}) \times (1 - \exp\{-a(31)[R_v - a(32)]^2\}) \tag{26}$$

$$A_4(R_k) = \prod_k B(1,0)\tanh\{a(33)[R_k - a(30)]\}. \tag{27}$$

In these equations, the $R_i$ run over all H–H vicinal distances. $R_u$ and $R_v$ are the Si–H distances of dissociating hydrogen atoms. The product function runs over the eight H–H distances from the two atoms forming $H_2$ to the remaining four hydrogen atoms. $B(1,0)$ is unity for positive values of the tanh function and zero otherwise.

The four-center dissociation terms include all possible four-center H–H vicinal interactions, each of which is described by a Morse potential. The $A_2$ attenuation function reduces these interactions to zero as the two Si–H bonds form to yield $Si_2H_6$. The $A_4$ function prevents the formation of hydrogen aggregates $H_n$ with $n > 2$.

The $V_{\mathrm{HH}}$ term in Eq. (3) is given by Eq. (25) for the $H_2$ molecule dissociated from $Si_2H_6$.

### 6. $V_{HH}^3$ term

The three-center $H_2$ dissociation terms have a form similar to that used for three-center dissociation in the $Si_2H_4$ potential-energy surface. $V_{\mathrm{HH}}^3$ includes all H–H interactions between hydrogens on the same silicon atom

$$V_{\mathrm{HH}}^3 = \sum_i V_{\mathrm{HH}}(R_i), \tag{28}$$

$$V_{\mathrm{HH}}(R_i) = a(28)(\exp\{-2a(29)[R_i - a(30)]\} - 2\exp\{-a(29)[R_i - a(30)]\}) \times A_3(R_u,R_v)A_5(R_n,R_m), \tag{29}$$

with

$$A_3(R_u,R_v) = 0.5(2 - \exp\{-a(34)[R_u - a(35)]^2\} - \exp\{-a(34)[R_v - a(35)]^2\}) \tag{30}$$

and

$$A_5(R_n,R_m) = B(1,0)\tanh\{a(33)[R_n - a(30)]\} \times \tanh\{a(33)[R_m - a(30)]\}. \tag{31}$$

In Eq. (28), the summation runs over all H–H distances

for hydrogen on the same silicon atom. $R_u$ and $R_v$ are the Si–H distances of the dissociating hydrogen atoms. $R_m$ and $R_n$ are the H–H distances from the two dissociating hydrogen atoms to the remaining hydrogen atom on the same silicon center.

The three-center dissociation terms include all possible three-center H–H interactions, each of which is described by a Morse potential. The $A_3$ attenuation function reduces these interactions to zero as the two Si–H bonds form to yield $Si_2H_6$. The $A_5$ function prevents the formation of $H_3$.

### 7. $V_T$ term

The $V_T$ term governs the transfer of a hydrogen atom in the dissociation channel leading to $SiH_2 + SiH_4$ products. It has the form

$$V_T = \sum_i V_{\mathrm{HT}}(R_i) + \sum_{i=13}^{30} V'_{\mathrm{H\text{-}Si\text{-}H}}(\theta_i), \tag{32}$$

where the first summation runs over the six vicinal Si–H distances in $Si_2H_6$. The hydrogen transfer terms $V_{\mathrm{HT}}$ are given by

$$V_{\mathrm{HT}}(R_i) = V_{\mathrm{SiH}}(R_i)A_6(R_1)S_4, \tag{33}$$

where $V_{\mathrm{SiH}}(R_i)$ is given by Eq. (10) and

$$A_6(R_1) = 1 - \exp\{-a(36)[R_1 - a(11)]^2\} \tag{34}$$

and

$$S_4 = \tanh\left[a(44)\left(4.5 - \sum_i \exp\{-a(43) \times [R_i - a(10)]^2\}\right)\right], \tag{35}$$

where the summation over $i$ runs over the distances between Si and the six hydrogen atoms.

The $A_6$ function requires the Si–Si bond to extend and break before a hydrogen atom can be transferred to form $SiH_2 + SiH_4$. The $S_4$ function prevents the transfer of a fifth hydrogen atom to form products such as $SiH + SiH_5$.

The $V'_{\mathrm{H\text{-}Si\text{-}H}}(\theta_i)$ terms are H–Si–H bending interactions for the $SiH_4$ molecule being formed in the hydrogen transfer reaction. Their functional form is identical to that given in Eqs. (19) and (20) except that the parameters $a(39)$, $a(40)$, and $a(41)$ replace $a(13)$, $a(17)$, and $a(12)$, respectively.

The only remaining term in the disilane potential surface is the $S_1$ switching function in Eq. (2), which controls the rate at which the disilane potential approaches that for $Si_2H_4$ as four-center $H_2$ dissociation occurs. Its functional form is

$$S_1(R_i,R_j) = \tanh\{a(38)[R_i - a(10)]^2[R_j - a(10)]^2\}, \tag{36}$$

where $R_i$ and $R_j$ are the two Si–H bond distances associated with the Si–H bonds being broken during the four-center dissociation process.

### 8. Adjustment of parameters

The $Si_2H_6$ potential contains 44 adjustable parameters plus those contained in the $Si_2H_4$ potential. The adjustment of the latter parameters has been described elsewhere.[4,5] Many of the $Si_2H_6$ parameters are adjusted so as to produce the correct geometries, fundamental vibrational frequencies, and energies for the stationary points on the $Si_2H_6$ surface as follows:

$a(1)$, $a(3)$, and $a(4)$ are adjusted to yield the Si–Si bond energies calculated by Ho *et al.*[18,19] $a(5)$, $a(6)$, $a(7)$, and $a(8)$ are adjusted to yield the calculated bond energies for Si–H bonds in $SiH_4$, $SiH_3$, $SiH_2$, and SiH. $a(10)$ and $a(11)$ are adjusted to the calculated Si–Si and Si–H equilibrium bond lengths, respectively. $a(13)$ adjusts the H–Si–H bond angle. $a(14)$–$a(16)$ and $a(27)$ are adjusted to give the equilibrium Si–Si–H bond angles for $Si_2H_6$ and $H_3Si$–SiH. $a(17)$ and $a(18)$ are determined by the measured fundamental vibration frequencies for the bending modes of $Si_2H_6$. The fundamental Si–Si stretching frequencies for $Si_2H_6$, $Si_2H_5$, and $H_3Si$–SiH determine the values of $a(20)$–$a(22)$. $a(23)$, $a(24)$, $a(25)$, and $a(26)$are adjusted by using the measured and calculated fundamental stretching frequencies for $Si_2H_6$ and $Si_2H_5$. $a(28)$–$a(30)$ are the Morse potential values for the H–H bond interaction. $a(37)$

TABLE I. $Si_2H_6$ potential-energy parameters.

| | | |
|---|---|---|
| $a(1)$ | = | 3.343 452 eV |
| $a(2)$ | = | 1.000 000 $A^{-2}$ |
| $a(3)$ | = | 2.637 034 eV |
| $a(4)$ | = | −0.215 308 eV |
| $a(5)$ | = | 3.337 381 eV |
| $a(6)$ | = | −0.212 056 eV |
| $a(7)$ | = | −0.102 342 eV |
| $a(8)$ | = | −0.060 350 eV |
| $a(9)$ | = | 1.000 000 $A^{-2}$ |
| $a(10)$ | = | 1.478 700 A |
| $a(11)$ | = | 2.363 000 A |
| $a(12)$ | = | 0.650 000 $A^{-2}$ |
| $a(13)$ | = | 1.895 951 rad |
| $a(14)$ | = | 1.925 098 rad |
| $a(15)$ | = | −0.005 700 |
| $a(16)$ | = | 1.500 000 $A^{-2}$ |
| $a(17)$ | = | 2.600 000 eV/rad$^2$ |
| $a(18)$ | = | 3.300 000 eV/rad$^2$ |
| $a(19)$ | = | 75.000 000 $A^{-2}$ |
| $a(20)$ | = | 1.420 000 $A^{-1}$ |
| $a(21)$ | = | 1.323 000 $A^{-1}$ |
| $a(22)$ | = | −0.015 500 $A^{-1}$ |
| $a(23)$ | = | 1.632 000 $A^{-1}$ |
| $a(24)$ | = | 0.000 000 $A^{-1}$ |
| $a(25)$ | = | −0.019 500 $A^{-1}$ |
| $a(26)$ | = | −0.015 700 $A^{-1}$ |
| $a(27)$ | = | 4.000 000 |
| $a(28)$ | = | 4.746 600 eV |
| $a(29)$ | = | 1.898 165 $A^{-1}$ |
| $a(30)$ | = | 0.741 900 A |
| $a(31)$ | = | 2.150 000 $A^{-2}$ |
| $a(32)$ | = | 1.478 000 A |
| $a(33)$ | = | 1.745 000 $A^{-1}$ |
| $a(34)$ | = | 2.250 000 $A^{-2}$ |
| $a(35)$ | = | 1.478 000 A |
| $a(36)$ | = | 0.850 000 $A^{-2}$ |
| $a(37)$ | = | 0.001 400 A |
| $a(38)$ | = | 0.300 000 $A^{-4}$ |
| $a(39)$ | = | 1.910 633 rad |
| $a(40)$ | = | 2.758 000 eV/rad$^2$ |
| $a(41)$ | = | 1.000 000 $A^{-2}$ |
| $a(42)$ | = | 5.200 000 $A^{-2}$ |
| $a(43)$ | = | 2.000 000 $A^{-2}$ |
| $a(44)$ | = | 8.000 000 |

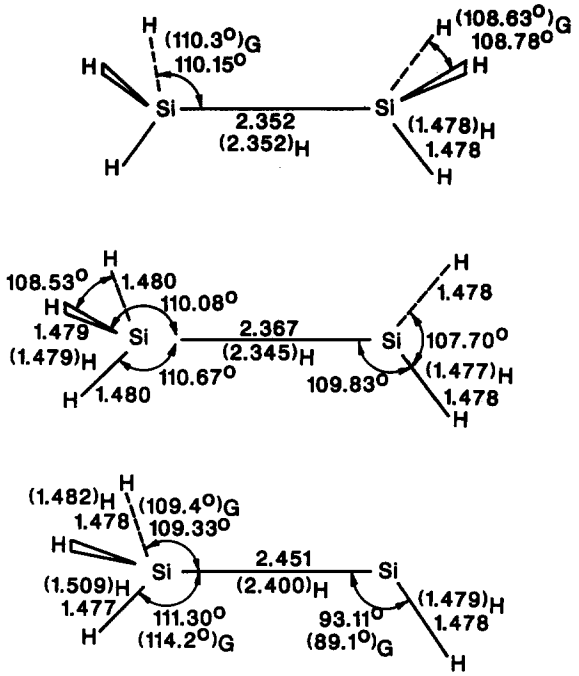


FIG. 3. Comparison of equilibrium bond lengths and angles given by Eq. (3) with those obtained from the *ab initio* calculations in Refs. 17–19. Numbers in parentheses labeled "G" refer to data from Ref. 17. Those labelled "H" refer to data from Refs. 18 and 19. Distances are given in angstroms and angles in degrees.

is used to obtain a more accurate Si–Si equilibrium bond distance for $H_3Si$–SiH. The equilibrium tetrahedral angle for $SiH_4$ is given by $a(39)$. The $SiH_4$ bending force constant is given by $a(40)$.

The remaining parameters are determined by adjustment of the barriers for the various reaction channels. $a(12)$, $a(36)$, $a(41)$, $a(42)$, $a(43)$, and $a(44)$ are used to adjust the variation along the reaction coordinate for the hydrogen-atom transfer channel leading to $SiH_2 + SiH_4$, so that the barrier to the back reaction is in near accord with that computed by Ho *et al.*[18,19] $a(31)$ and $a(38)$ are used in a similar manner to adjust the barrier for the four-center $H_2$ dissociation channel. $a(19)$, $a(34)$, and $a(35)$ are employed to adjust the reaction coordinate for three-center $H_2$ dissociation. $a(32)$ is taken to be the equilibrium Si–H distance in $Si_2H_6$. $a(33)$ is set to the value obtained in our previous study of the $Si_2H_4$ potential surface. In that case, this parameter was used to obtain the correct barrier height for the $H + H_2$ exchange reaction.

The parameters $a(2)$ and $a(9)$ determine attenuation rates. These values are arbitrarily set to unity. The values of all parameters are given in Table I.

TABLE II. Calculated equilibrium bond lengths for various $Si_nH_m$ molecules. All distances are given in angstroms.

| Molecule | Bond | Length | |
|---|---|---|---|
| | | Equation (3) | Ho *et al.*[a] |
| $Si_2H_6$ | Si–H | 1.479 | 1.478 |
| | Si–Si | 2.381 | 2.352 |
| $Si_2H_5$ | Si–H | 1.480 ($SiH_3$) | 1.479 |
| | | 1.480 ($SiH_3$) | |
| | | 1.479 ($SiH_3$) | |
| | | 1.479 ($SiH_2$) | 1.477 |
| | Si–Si | 2.395 | 2.345 |
| $H_3Si$–SiH | Si–H | 1.476 ($SiH_3$) | 1.482 |
| | | 1.476 ($SiH_3$) | 1.482 |
| | | 1.479 ($SiH_3$) | 1.509 |
| | | 1.478 (SiH) | 1.479 |
| | Si–Si | 2.479 | 2.400 |
| $SiH_3$ | Si–H | 1.479 | 1.476[b] |

[a] Reference 19.
[b] Reference 17.

## C. Properties of the surface

### 1. Equilibrium geometries

The equilibrium structures and corresponding energies for the reactants and products of reactions (R1)–(R6) have been determined from the results of damped trajectories. The general procedure used in these studies has been previously described.[13] Figure 3 shows the predicted equilibrium geometries for disilane, $Si_2H_5$, and $H_3Si$–SiH. These are compared with the *ab initio* results obtained by Coltrin *et al.*[18,19] and by Gordon *et al.*[17] In each case, the *ab initio* results are given in parentheses beside the value obtained from the empirical surface. Subscripts "H" and "G" denote values obtained by Ho *et al.*[18,19] and Gordon *et al.*,[17] respectively. Table II gives a comparison of the equilibrium bond lengths given by Eq. (3) with those reported by Ho *et al.*[18,19] A similar comparison for the equilibrium bond angles obtained from Eq. (3) with those computed by Gordon *et al.*[17] is given in Table III. In general, equilibrium bond lengths are predicted within 0.01 A or better. Most of the equilibrium angles are within 2° of the *ab initio* results. Only the unusually small Si–Si–H bond angle in $H_3Si$–SiH has an error greater than 3°.

### 2. Reaction endothermicities/exothermicities

Table IV gives the predicted heats of reaction for 13 reactions involving disilane or molecules derived from disi-

TABLE III. Calculated equilibrium bond angles for various $Si_nH_m$ molecules. All angles are given in degrees.

| Molecule | Bond angle | Equation (3) | Gordon *et al.*[a] |
|---|---|---|---|
| $Si_2H_6$ | Si–Si–H | 110.8 | 110.3 |
| | H–Si–H | 108.1 | 108.63 |
| $Si_2H_5$ | Si–Si–H | 111.4 ($SiH_3$) | ··· |
| | | 111.4 ($SiH_3$) | ··· |
| | | 109.7 ($SiH_3$) | ··· |
| | | 110.8 ($SiH_2$) | ··· |
| $H_3Si$–SiH | Si–Si–H | 108.7 ($SiH_3$) | 109.4 |
| | | 108.7 ($SiH_3$) | 109.4 |
| | | 113.2 ($SiH_3$) | 114.2 |
| | | 95.3 (SiH) | 89.1 |
| | H–Si–H | 108.7 | 107.8 |
| $SiH_3$ | H–Si–H | 108.6 | 111.1 |

[a] Reference 17.

TABLE IV. Calculated heats of reaction for various reactions of disilane or molecules derived from disilane. The results are given in units of kcal/mol.

| Reaction | Equation (3) | Ho *et al.*[a] | Experimental[b] | Reference Nos. |
|---|---|---|---|---|
| $Si_2H_6 \rightarrow Si_2H_5 + H$ | 88.6 | 88.7 | 86.3 | 23–25 |
| $Si_2H_6 \rightarrow 2SiH_3$ | 75.9 | 76.5 | 79.1 | 26,27 |
| | | | 73.1 | 25 |
| | | | 76.1 | 28 |
| $Si_2H_6 \rightarrow H_3Si\text{–}SiH + H_2$ | 60.3 | 61.3 | 49.8 | 15(c) |
| | | | 46.1 | 16 |
| $Si_2H_6 \rightarrow SiH_2 + SiH_4$ | 56.8 | 57.8 | 57.7 | 24,28,29 |
| | | | 57.8 | 23–25 |
| | | | 60.0 | 28 |
| $Si_2H_6 \rightarrow H_2Si = SiH_2 + H_2$ | 30.5 | 38.0 | 38.9 | 30 |
| $Si_2H_5 \rightarrow H_3Si\text{–}SiH + H$ | 81.0 | 76.8 | 67.7 | 15(c),23–25 |
| | | | 64.0 | 16,23–25 |
| $Si_2H_5 \rightarrow H_2Si = SiH_2 + H$ | 51.1 | 53.5 | 56.8 | 23–25,30 |
| $H_3Si\text{–}SiH \rightarrow H_2Si = SiH + H$ | 71.3 | 77.5 | ··· | |
| $H_3Si\text{–}SiH \rightarrow H_2Si = Si + H_2$ | 12.7 | 24.0 | ··· | |
| $H_2Si = SiH_2 \rightarrow H_2Si = SiH + H$ | 101.1 | 100.8 | ··· | |
| $H_2Si = SiH_2 \rightarrow H_2Si = Si + H_2$ | 42.5 | 47.3 | ··· | |
| $H_3Si\text{–}SiH \rightarrow H_2Si = SiH_2$ | −29.9 | −23.3 | −10.9 | 15(c),30 |
| | | | −7.2 | 16,30 |
| $H_2Si = SiH \rightarrow H_2Si = Si + H$ | 50.7 | 50.7 | ··· | |

[a] References 18 and 19.
[b] Values are computed from estimated heats of formation obtained from the references cited.

lane. These are compared with the values obtained from the MP4 calculations reported by Ho *et al.*[18,19] and with the available experimental data. The average absolute difference between the results obtained with Eq. (3) and the MP4 calculations for all reactions is 3.55 kcal/mol, which corresponds to an average percent absolute difference of 9.83%. The majority of this difference is the result of an 11.3 kcal/mol variation in the predicted endothermicity for four-center $H_2$ dissociation from $H_3Si\text{–}SiH$. If this reaction is omitted, the average absolute difference for the remaining 12 reactions given in Table IV is 2.90 kcal/mol, which corresponds to an average percent difference of 6.83%.

The average absolute difference between the results obtained from Eq. (3) and the heats of reaction estimated from heats of formation obtained from various measurements is 6.33 kcal/mol. Most of this difference is the result of the heat of formation of $H_3Si\text{–}SiH$. Using kinetic data from trisilane pyrrolysis, White *et al.*[15(c)] estimate this value to be 68.9 kcal/mol. Walsh *et al.*[16] have obtained a value of 65.2 kcal/mol from the results of decomposition studies of chemically activated disilane. Both of these values are considerably lower than the 80.4 kcal/mol value obtained from the MP4 calculations[19] to which the empirical surface is fitted. If reactions involving $H_3Si\text{–}SiH$ are omitted, the average absolute difference between the results obtained from Eq. (3) and the experimentally derived values is 3.01 kcal/mol.

### 3. Fundamental vibration frequencies

Harmonic normal-mode frequencies have been obtained by numerical computation of the second derivative force constant matrix using Eq. (3). Table V lists the results for disilane. The results for $Si_2H_5$ and $H_3Si\text{–}SiH$ are given in Tables VI and VII, respectively.

As can be seen, the predicted frequencies for disilane are generally in good accord with the measured values. The average absolute error for all modes is 58.7 $cm^{-1}$. Modes 2 and 3 are exceptions. It is difficult for the empirical surface to correctly predict all of the Si–Si–H deformation mode frequencies since Eq. (3) contains only one force constant for this bending motion. Better agreement could be obtained by expansion of Eq. (22) to include a second type of bending force.

The results for $Si_2H_5$ are similar to those obtained for

TABLE V. Calculated fundamental vibration frequencies for disilane. Units are $cm^{-1}$.

| Mode | Symmetry | Equation (3) | Experimental[a] |
|---|---|---|---|
| 1 | $A_{1u}$ | 91 | 120.48[b] |
| 2 | $E_u$ | 630 | 379 |
| 3 | $E_u$ | 630 | 379 |
| 4 | $A_{1g}$ | 403 | 432 |
| 5 | $E_g$ | 677 | 628 |
| 6 | $E_g$ | 677 | 628 |
| 7 | $A_{2u}$ | 947 | 844 |
| 8 | $E_g$ | 930 | 941 |
| 9 | $E_g$ | 930 | 941 |
| 10 | $A_{1g}$ | 964 | 920 |
| 11 | $E_u$ | 976 | 940 |
| 12 | $E_u$ | 976 | 940 |
| 13 | $A_{2u}$ | 2165 | 2154 |
| 14 | $E_g$ | 2202 | 2155 |
| 15 | $E_g$ | 2202 | 2155 |
| 16 | $E_u$ | 2204 | 2179 |
| 17 | $E_u$ | 2204 | 2179 |
| 18 | $A_{1g}$ | 2166 | 2163 |

[a] J. R. Durig and J. S. Church, J. Chem. Phys. 73, 4784 (1980).
[b] Reference 19.

TABLE VI. Calculated fundamental vibration frequencies for $Si_2H_5$. Units are $cm^{-1}$.

| Mode | Equation (3) | Ho *et al.*[a] |
|---|---|---|
| 1 | 85 | 116 |
| 2 | 330 | 389 |
| 3 | 534 | 423 |
| 4 | 640 | 429 |
| 5 | 641 | 614 |
| 6 | 721 | 633 |
| 7 | 934 | 881 |
| 8 | 949 | 929 |
| 9 | 951 | 940 |
| 10 | 968 | 941 |
| 11 | 2107 | 2135 |
| 12 | 2138 | 2147 |
| 13 | 2143 | 2147 |
| 14 | 2196 | 2158 |
| 15 | 2222 | 2158 |

[a] Reference 19.

$Si_2H_6$. Again, there are problems with the low-frequency deformation modes 3 and 4. The frequencies for these modes are too high by 111 and 211 $cm^{-1}$, respectively. As in the case of $Si_2H_6$, this is a consequence of using only one force constant for the Si–Si–H bending motions. Otherwise, the degree of agreement with the *ab initio* calculations[18,19] is satisfactory. The average absolute difference between these results is 52.1 $cm^{-1}$.

The normal-mode frequencies given by Eq.(3) for $H_3Si$–SiH are also in good accord with the *ab initio* results[18,19] except for the low-frequency deformations, modes 3 and 4 in Table VII. The average absolute difference here is 62.8 $cm^{-1}$.

Finally, we note that the number of normal-mode frequencies present for $Si_2H_6$ is significantly greater than the number of parameters available in Eq. (3) for adjustment to these frequencies. Furthermore, there was no adjustment attempted for $H_3Si$–SiH and very little for $Si_2H_5$. Nevertheless, the accuracy obtained for these latter two molecules is comparable to that for disilane. In part, this is a consequence of our use of physically and chemically motivated functional forms in Eq. (3). It is doubtful whether a series expansion in terms of arbitrary functions could have achieved such a result.

TABLE VII. Calculated fundamental vibration frequencies for $H_3Si$–SiH. Units are $cm^{-1}$.

| Mode | Equation (3) | Ho *et al.*[a] |
|---|---|---|
| 1 | 85 | 112 |
| 2 | 299 | 380 |
| 3 | 610 | 401 |
| 4 | 619 | 433 |
| 5 | 725 | 724 |
| 6 | 917 | 887 |
| 7 | 941 | 926 |
| 8 | 959 | 945 |
| 9 | 2058 | 2005 |
| 10 | 2090 | 2126 |
| 11 | 2100 | 2127 |
| 12 | 2220 | 2146 |

[a] Reference 19.

TABLE VIII. Potential barrier heights for various reactions of disilane. Units are in kcal/mol.

| Reaction | Equation (3) (eV) | Ho *et al.*[a] |
|---|---|---|
| $Si_2H_6 \rightarrow SiH_2 + SiH_4$ | 56.8 | 57.9 |
| $Si_2H_6 \rightarrow H_2Si = SiH_2 + H_2$ | 91.1 | 91.1 |
| $Si_2H_6 \rightarrow H_3Si$–SiH + $H_2$ | 60.3 | 61.3 |

[a] Reference 19.

### 4. Reaction profiles and barrier heights

The reaction profiles and barrier heights for the following reactions have been determined:

$$Si_2H_6 \rightarrow [H_2Si\text{--}\,\text{--}H\text{–}SiH_3] \rightarrow SiH_2 + SiH_4,$$

$$H_3Si\text{–}SiH_3 \rightarrow \begin{bmatrix} H_2Si\text{--}\,\text{--}SiH_2 \\ \\ H\text{--}\,\text{--}H \end{bmatrix} \rightarrow H_2Si = SiH_2 + H_2,$$

$$H_3Si\text{–}SiH_3 \rightarrow \begin{bmatrix} & & H \\ H_3Si\text{–}SiH & & \\ & & H \end{bmatrix} \rightarrow H_3Si\text{–}SiH + H_2.$$

For the reaction leading to $SiH_2 + SiH_4$, we assume that the reaction pathway involves a hydrogen-atom transfer in the plane containing the hydrogen and the two silicon atoms. The actual path is determined by the incremental displacement of hydrogen in the direction that minimizes the change in the potential energy. After displacement, the Si–Si distance is adjusted to minimize the potential. Finally, the five nontransferring hydrogen atoms are allowed to relax to their most stable conformations. For the four-center $H_2$ elimina-

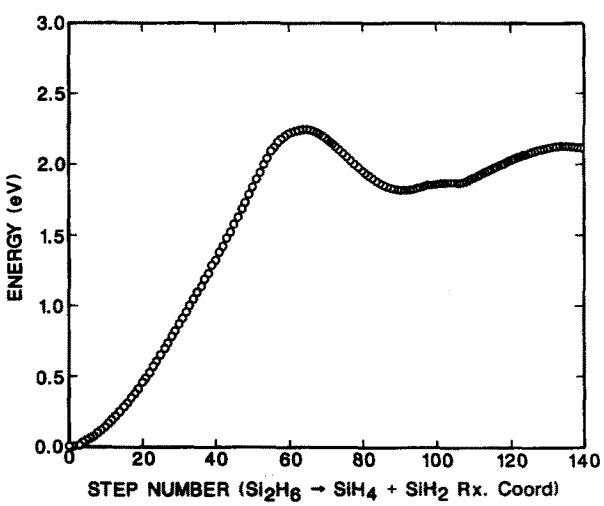


FIG. 4. Reaction profile for the hydrogen transfer reaction leading to $SiH_4 + SiH_2$ products. Disilane in its equilibrium configuration is taken as the energy zero. Each step on the abscissa corresponds to a displacement of the transferring hydrogen atom by 0.05 Å along the pathway described in the text.

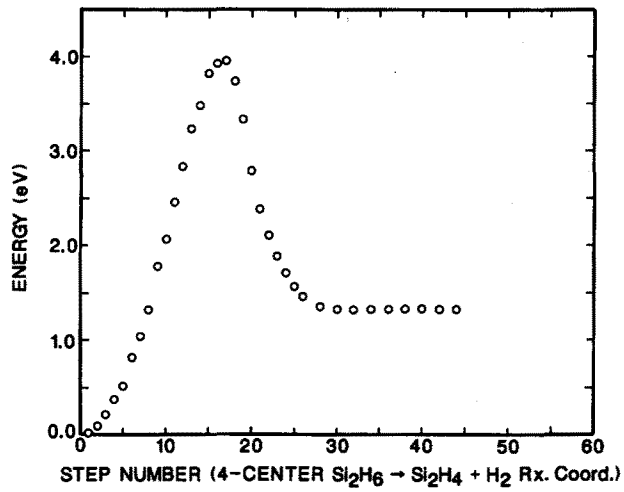


FIG. 5. Reaction profile for the planar four-center $H_2$ abstraction reaction. Disilane in its equilibrium configuration is taken as the energy zero. Each step on the abscissa corresponds to a displacement of 0.10 Å along the four-center pathway described in the text and in Ref. 5.

tion, it was assumed that dissociation occurs along a pathway in which the silicon atoms and the dissociating hydrogen atoms lie in a plane. The four nondissociating hydrogen atoms were allowed to relax to their most stable configurations at each point along the reaction coordinate. For the symmetric, three-center dissociation reaction, the second silicon atom and the four nondissociating hydrogen atoms were allowed to relax at each step.

The results for the barrier heights are compared with the *ab initio* values obtained by Ho *et al.*[18,19] in Table VIII. The reaction profile for the $SiH_2 + SiH_4$ transfer reaction is shown in Fig. 4. Figure 5 shows the reaction profile for four-center hydrogen dissociation while Fig. 6 gives that for three-center hydrogen dissociation. In general, the extent of agreement with the *ab initio* results is excellent in all cases. It should be noted, however, that there is no guarantee that the pathway considered for four-center elimination is that corresponding to the minimum-energy path. In fact, we have some evidence from our previous studies of the dynamics for $Si_2H_4$ decomposition[5] that lower-energy pathways exist. Consequently, the data given in Table VIII for reaction (R6) should be regarded as an upper limit for the reaction barrier height on the potential surface given by Eq. (3). At the internal energies considered in this paper, this high-barrier reaction is of virtually no importance in the overall decomposition dynamics of disilane.

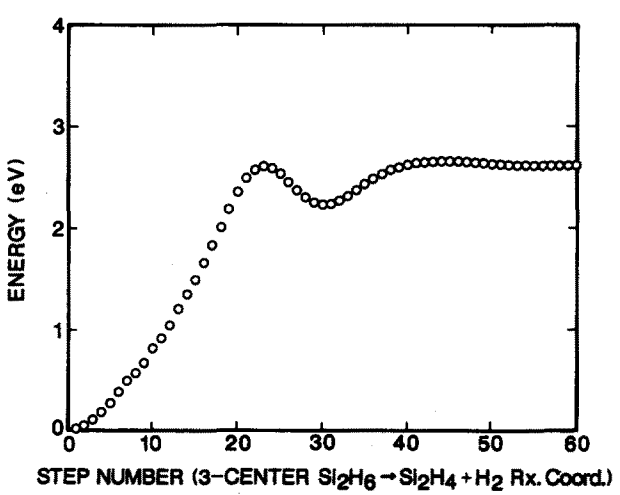


FIG. 6. Reaction profile for the three-center $H_2$ abstraction reaction. Disilane in its equilibrium configuration is taken as the energy zero. Each step on the abscissa corresponds to a displacement of 0.05 Å along the three-center pathway described in the text and in Ref. 5.

## III. DISSOCIATION DYNAMICS

### A. Methods

The unimolecular dissociation rates and dynamics for reactions (R2)–(R6) on the potential-energy surface described in Sec. II have been computed from the results of classical trajectory calculations.[20] The decomposition dynamics have been investigated for seven values of the total $Si_2H_6$ internal energy ranging from 5.31 to 9.31 eV, including the 1.31 eV of zero-point energy. Batches of 100 trajectories were computed at each energy equal to or greater than 6.81 eV. For internal energies less than 6.81 eV, where the decomposition rates are significantly slower, batches of 200 trajectories were computed at each energy. The number of dissociating trajectories per batch varies from 34 to 97 except at the lowest energy studied 5.31 eV, where only 11 trajectories undergo decomposition.

Initial-state averaging is carried out using projection methods.[21,22] With disilane in its ground-state equilibrium geometry, zero-point energy is inserted into each of the normal modes. A trajectory is then run for a time $t_i$ that is sufficient to redistribute the internal energy between potential and kinetic modes. At time $t_i$, the difference between the desired total energy and the zero-point energy is equipartitioned and inserted into the normal modes as described in Ref. 22. Initial phase averaging is accomplished by choosing $t_i$ randomly over a time equal to one vibrational period for a mode with median vibrational frequency for $Si_2H_6$.

Numerical integration was done using a Runga–Kutta method with a fixed step of 0.02 t.u. (1 t.u. $= 1.019 \times 10^{-14}$ s). The trajectory is evolved for 60 t.u. or until dissociation occurs.

The total disilane dissociation rate coefficient $k_T$ is given by

$$k_T = k_2 + k_3 + k_4 + k_5 + k_6, \tag{37}$$

where $k_i$ is the dissociation rate coefficient for reaction Ri, provided the total dissociation process of $Si_2H_6$ may be described by the competing series of concurrent reactions (R2)–(R6). If each of these reactions is a first-order process, then we have

$$\ln[N/N_0] = -k_T t, \tag{38}$$

where $N$ is the total number of undissociated trajectories at time $t$ and $N_0$ is the total number of trajectories computed. $k_T$ values at each internal energy are obtained from the slope of a plot of $\ln[N/N_0]$ vs time. A typical decay plot for $E = 8.31$ eV is shown in Fig. 7. The rate coefficient for each dissociation channel is obtained from the total number of

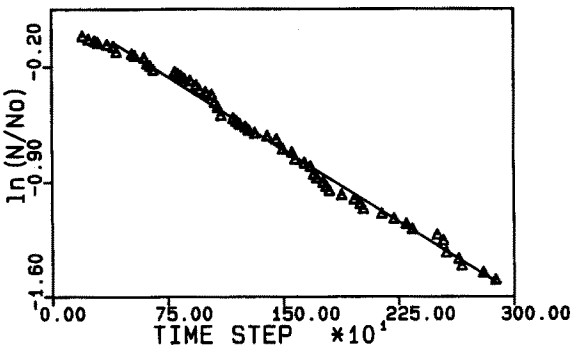


FIG. 7. $\ln[N/N_0]$ vs time step for the unimolecular dissociation of disilane at a total internal energy of 8.31 eV. The straight line is the linear least-squares fit to the trajectory data given by the triangles. One time step is $2.038\times10^{-16}$ s.

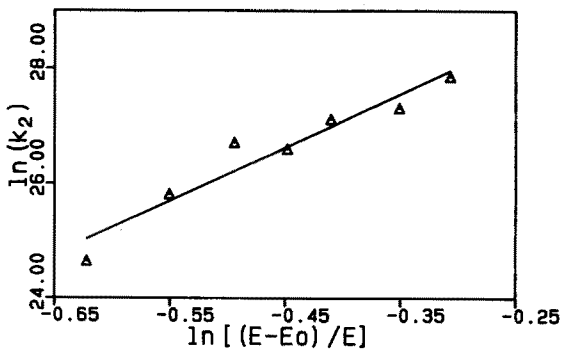


FIG. 8. RRK plot of the rate coefficients for reaction (R2). The rate coefficients are given in $s^{-1}$. The straight line is a linear least-squares fit to the trajectory data given by the triangles.

dissociations into that channel

$$k_i = [N_i/(N_0 - N)]k_T, \tag{39}$$

where $N_i$ is the total number of trajectories observed to dissociate into the $i$th channel.

### B. Rate coefficients and energy partitioning

Table IX gives the computed Values of $k_2$–$k_6$ as a function of total internal $Si_2H_6$ energy. At low internal energy, the dissociation channel leading to $SiH_4$ and $SiH_2$ dominates the dynamics. This result is in accord with the experimental data reported by Purnell *et al.*[14] and by Ring *et al.*[15] which fail to find any evidence for radical production. Such a result is not unexpected since reaction (R2) has the lowest potential barrier of any of the dissociation channels on our potential-energy surface.

As the internal energy increases, however, Si–Si bond cleavage and three-center $H_2$ elimination begin to compete favorably with dissociation to $SiH_4 + SiH_2$. At sufficiently high internal energy, Si–Si bond rupture becomes the major decomposition pathway and three-center $H_2$ elimination competes favorably for second place. This behavior is due to a competition between energy and entropy effects in the different dissociation channels. Energy considerations favor decomposition to form $SiH_4 + SiH_2$. However, since more of the vibrational modes of $Si_2H_6$ are coupled to the coordinate leading to reaction (R2), entropy effects tend to decrease the rate of this process. In contrast, the relatively high barrier for Si–Si bond rupture tends to slow reaction (R3), but since fewer vibrational modes are coupled to the Si–Si stretching mode, entropy effects tend to enhance the chances for decomposition via this channel. Consequently, as the energy increases, the differences in barrier height become less significant and entropy effects invert the relative importance of channels (R2) and (R3).

The above concepts may be quantified by expressing the energy dependence of the rate coefficients in RRK form

$$k(E) = f[(E - E_0)/E]^{s-1}. \tag{40}$$

Here, $k(E)$ is the rate coefficient at internal energy $E$ and $E_0$ is the critical energy that can be taken to be equal to the barrier height of the reaction, $f$ is the frequency factor or high-energy limit of the rate coefficient, and $s$ is a parameter related to the number of internal degrees of freedom participating in the reaction. Graphs showing the variation of $\ln[k(E)]$ as a function of $\ln[(E - E_0)/E]$ for reactions (R2)–(R5) are shown in Figs. 8–11.The values of $s$ and $f$ derived from the linear least-squares fits of the trajectory data are given in Table X along with the values of $E_0$ obtained from the potential-energy surface.

Qualitatively, the values of the frequency factor are re-

TABLE IX. Microcanonical rate coefficients for different dissociation channels of disilane. Rate coefficients are given in units of $10^{12}$ $s^{-1}$.

| Energy (eV) | $k_2$ | $k_3$ | $k_4$ | $k_5$ | $k_6$ |
|---|---|---|---|---|---|
| 9.31 | 1.25 | 2.07 | 1.69 | 0.75 | 0.31 |
| 8.31 | 0.73 | 1.03 | 0.88 | 0.27 | $x^a$ |
| 7.31 | 0.60 | 0.46 | 0.49 | 0.057 | $x$ |
| 6.81 | 0.36 | 0.30 | 0.42 | 0.060 | 0.06 |
| 6.31 | 0.40 | 0.23 | 0.23 | 0.037 | $x$ |
| 5.81 | 0.16 | 0.15 | 0.07 | 0.012 | $x$ |
| 5.31 | 0.051 | 0.025 | 0.017 | $x$ | $x$ |

[a] The notation $x$ means no trajectories were observed to dissociate into this channel within $0.6114\times10^{-12}$ s.

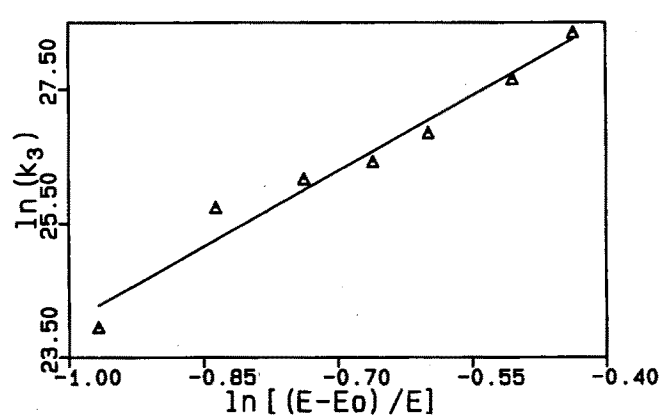


FIG. 9. RRK plot of the rate coefficients for reaction (R3). The rate coefficients are given in $s^{-1}$. The straight line is a linear least-squares fit to the trajectory data given by the triangles.

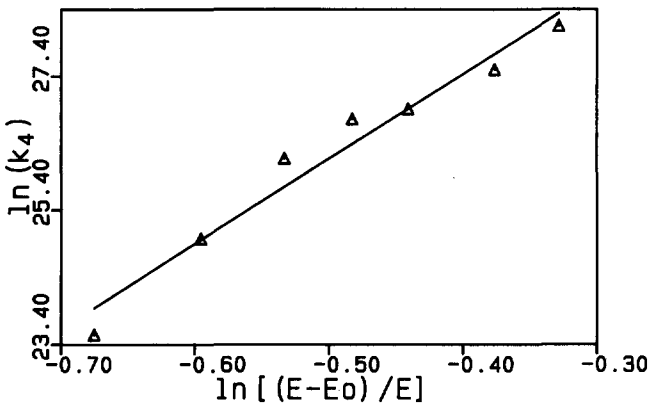


FIG. 10. RRK plot of the rate coefficients for reaction (R4). The rate coefficients are given in $s^{-1}$. The straight line is a linear least-squares fit to the trajectory data given by the triangles.

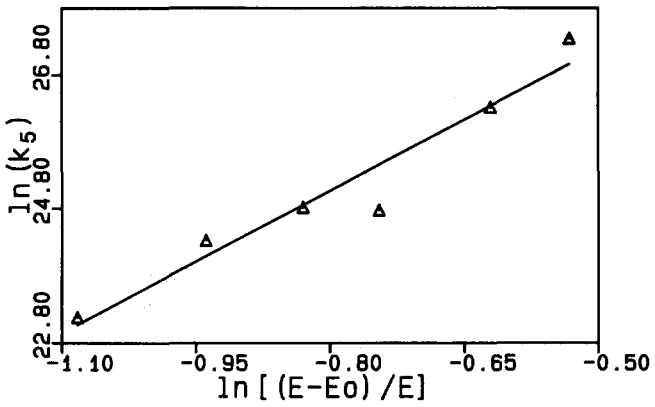


FIG. 11. RRK plot of the rate coefficients for reaction (R5). The rate coefficients are given in $s^{-1}$. The straight line is a linear least-squares fit to the trajectory data given by the triangles.

lated to entropy effects, the vibrational frequencies of the modes most directly responsible for reaction, and the number of possible ways in which the reaction in question can occur, e.g., reaction (R4) can take place by the combination of six different pairs of hydrogen atoms, whereas reaction (R3) can occur in only one way. Since $s$ approximates the number of vibrational modes coupled to the reaction coordinate, a large value of $s$ will lead to greater entropy effects. That is, if the value of $s$ is large, the internal energy available to move the system along that particular reaction coordinate will tend to spread over more internal degrees of freedom thereby reducing the probability that a particular coordinate will attain the requisite energy $E_0$ for decomposition.

The data given in Table X support the qualitative concepts described above. The $s$ value for reaction (R3) is significantly lower than that for reaction (R2). Consequently, we expect fewer modes to be coupled to the Si–Si bond rupture reaction coordinate which will, in turn, reduce the entropy effects in this reaction. In contrast, the three-center $H_2$ elimination channel has an $s$ value of 13.69 suggesting the coupling of most of the $Si_2H_6$ modes to this reaction coordinate. We have previously noted similar behavior for three-center $H_2$ elimination from $Si_2H_4$, where an $s$ value of 11.2 was obtained.[5] Nevertheless, reaction to produce $H_3Si$–SiH competes favorably with reaction (R2) at sufficiently high internal energy. This is primarily because of the much larger frequency factor for $H_2$ elimination than for reactions that involve Si–Si bond rupture.

The data given in Table X shows four-center elimination to be a slow process relative to reactions (R2)–(R5). Experimentally, it is found that substantial quantities of $H_2Si=SiH_2$ are formed in the decomposition reactions of $Si_2H_6$. Ring *et al.*[15] and Walsh *et al.*[16] have suggested that $H_2Si=SiH_2$ is formed in a direct decomposition reaction of disilane. On the other hand, Ho *et al.*[19] postulate that the route to disilene leads through $H_3Si$–SiH formed by three-center elimination of $H_2$ followed by a low-barrier, fast hydrogen transfer reaction to form $H_2Si=SiH_2$. The high yields of $H_3Si$–SiH obtained in the present study, coupled with the near absence of four-center reactions even at energies in substantial excess of the critical energies support this view.

The distribution of energy among the translational, vibrational, and rotational degrees of freedom of the products is given in Table XI. As expected, most of the available energy (65% to 81%) is partitioned into vibrational motion. In general, the energy partitioning is governed by statistical considerations. Translational and rotational motion are associated with three and six degrees of freedom, respectively, for the products of reactions (R2) and (R3) and with three and five, respectively, for reaction (R4). Consequently, if statistical considerations alone determined the energy partitioning, we would expect the ratio of translational to rotational energy for reactions (R2) and (R3) to be 1:2 and 3:5 for reaction (R4). The trajectory data for reactions (R2) and (R3) agree fairly well with this prediction. The three-center dissociation channel (R4), however, has a translation-to-rotation ratio nearly equal to unity or greater. In this case, dynamic effects clearly play a more important role. If the energy were partitioned equally among all modes, the ratio of translational-to-total energy would be 0.143. The results for all reactions show this fraction to be about $(0.10 \pm 0.08)$.

An examination of the internal energy distribution shows that the fraction of energy partitioned into rotation tends to decrease while that present as product vibration tends to increase as the total energy of the system increases. Similar behavior has also been found for unimolecular reactions of $Si_2H_4$.[5] This trend may be the result of the increase

TABLE X. RRK parameters for reactions (R2), (R3), (R4), and (R5).

| Reaction | $E_0$ (eV) | $f^a$ | $s$ |
|---|---|---|---|
| (R2) | 2.46 | 0.237 | 10.26 |
| (R3) | 3.29 | 0.492 | 8.49 |
| (R4) | 2.61 | 1.316 | 13.69 |
| (R5) | 3.84 | 0.219 | 8.06 |

[a] $f$ is given in units of $10^{14}$ $s^{-1}$.

TABLE XI. Distribution of energy among the products of different dissociation channels of disilane. $\langle F_T \rangle$, $\langle F_R \rangle$, and $\langle F_V \rangle$ denote the average fractions of the available energy partitioned into translation, rotation, and vibration, respectively. The statistical uncertainties are given by $\pm$ the values in parentheses.

| Reaction | Energy (eV) | $\langle F_T \rangle$ | $\langle F_R \rangle$ | $\langle F_V \rangle$ |
|---|---|---|---|---|
| (R2) | 9.31 | 0.08(0.06) | 0.15(0.05) | 0.77(0.09) |
| | 8.31 | 0.14(0.11) | 0.12(0.06) | 0.74(0.14) |
| | 7.31 | 0.09(0.09) | 0.18(0.07) | 0.72(0.10) |
| | 6.81 | 0.09(0.06) | 0.21(0.11) | 0.70(0.12) |
| | 6.31 | 0.12(0.12) | 0.19(0.08) | 0.69(0.12) |
| | 5.81 | 0.09(0.05) | 0.20(0.07) | 0.71(0.05) |
| (R3) | 9.31 | 0.07(0.06) | 0.17(0.08) | 0.76(0.12) |
| | 8.31 | 0.07(0.07) | 0.20(0.08) | 0.73(0.10) |
| | 7.31 | 0.07(0.03) | 0.20(0.08) | 0.73(0.09) |
| | 6.81 | 0.07(0.05) | 0.26(0.04) | 0.67(0.07) |
| | 6.31 | 0.14(0.11) | 0.21(0.13) | 0.65(0.13) |
| | 5.81 | 0.10(0.10) | 0.24(0.10) | 0.66(0.11) |
| (R4) | 9.31 | 0.14(0.08) | 0.08(0.07) | 0.78(0.09) |
| | 8.31 | 0.14(0.09) | 0.07(0.07) | 0.79(0.10) |
| | 7.31 | 0.15(0.07) | 0.10(0.08) | 0.75(0.12) |
| | 6.81 | 0.12(0.07) | 0.14(0.13) | 0.75(0.15) |
| | 6.31 | 0.08(0.06) | 0.11(0.08) | 0.81(0.08) |
| | 5.81 | 0.15(0.03) | 0.14(0.06) | 0.71(0.08) |
| (R5) | 9.31 | 0.10(0.08) | 0.13(0.09) | 0.77(0.10) |
| | 8.31 | 0.10(0.09) | 0.14(0.09) | 0.76(0.11) |
| | 7.31 | 0.10(0.08) | 0.16(0.09) | 0.74(0.10) |
| | 6.81 | 0.09(0.06) | 0.19(0.12) | 0.72(0.13) |
| | 6.31 | 0.12(0.11) | 0.18(0.11) | 0.70(0.13) |
| | 5.81 | 0.11(0.08) | 0.20(0.09) | 0.69(0.09) |

in the average molecular moments of inertia that occurs with an increase in the vibrational energy.

Tables XII and XIII give an analysis of the energy partitioning for different products in reactions (R2) and (R3), respectively. The sharing of translational energy in the ratio of masses is trivial. The rotational energies of $SiH_4$ and $SiH_2$ in reaction (R2) are almost equal as would be expected from statistical considerations. Such a result also suggests that the decomposition mechanism is such that any torque imparted to $SiH_4$ in the transfer process would also be imparted to the $SiH_2$ product. In contrast, the rotational energy of $H_2$ in three-center elimination reactions is much larger than would be expected from statistical arguments alone. Similar results have also been obtained for three-center $H_2$ elimination reactions from $Si_2H_4$.[5] This result leads us to suggest that the

TABLE XII. Distribution of available energy among different products of dissociation of disilane into channel (R2). $\langle F_T \rangle$, $\langle F_R \rangle$, and $\langle F_V \rangle$ denote fractions of the available energy partitioned into translation, rotation, and vibration, respectively.

| | $\langle F_T \rangle$ | | $\langle F_R \rangle$ | | $\langle F_V \rangle$ | |
|---|---|---|---|---|---|---|
| Energy (eV) | $SiH_4$ | $SiH_2$ | $SiH_4$ | $SiH_2$ | $SiH_4$ | $SiH_2$ |
| 9.31 | 0.04 | 0.04 | 0.09 | 0.06 | 0.68 | 0.09 |
| 8.31 | 0.07 | 0.07 | 0.05 | 0.07 | 0.62 | 0.12 |
| 7.31 | 0.05 | 0.05 | 0.10 | 0.09 | 0.56 | 0.16 |
| 6.81 | 0.04 | 0.04 | 0.12 | 0.09 | 0.53 | 0.17 |
| 6.31 | 0.06 | 0.06 | 0.11 | 0.08 | 0.61 | 0.08 |
| 5.81 | 0.04 | 0.04 | 0.11 | 0.09 | 0.50 | 0.21 |

TABLE XIII. Distribution of available energy among different products of dissociation of disilane into channel (R4). $\langle F_T \rangle$, $\langle F_R \rangle$, and $\langle F_V \rangle$ denote fractions of the available energy partitioned into translation, rotation, and vibration, respectively.

| | $\langle F_T \rangle$ | | $\langle F_R \rangle$ | | $\langle F_V \rangle$ | |
|---|---|---|---|---|---|---|
| Energy (eV) | $H_3Si$–$SiH$ | $H_2$ | $H_3Si$–$SiH$ | $H_2$ | $H_3Si$–$SiH$ | $H_2$ |
| 9.31 | 0.005 | 0.14 | 0.012 | 0.07 | 0.71 | 0.07 |
| 8.31 | 0.004 | 0.13 | 0.014 | 0.06 | 0.64 | 0.15 |
| 7.31 | 0.005 | 0.14 | 0.018 | 0.08 | 0.61 | 0.15 |
| 6.81 | 0.004 | 0.11 | 0.016 | 0.12 | 0.62 | 0.12 |
| 6.31 | 0.003 | 0.08 | 0.015 | 0.10 | 0.73 | 0.08 |
| 5.81 | 0.005 | 0.15 | 0.029 | 0.11 | 0.63 | 0.08 |

average reaction pathway probably does not correspond to a symmetric $H_2$ elimination. The large $H_2$ rotational energy requires asymmetric dissociation that provides torque and angular momenta to the departing $H_2$ molecule.

The vibrational partitioning data in Tables XII and XIII indicate that, on average, $SiH_4$ and $H_2$ contain more vibrational energy than would be expected from statistical considerations alone. This is not unexpected since new bonds must be formed to produce these two molecules. In general, unimolecular products that have had new bonds formed in their production will contain more than a statistical amount of vibrational energy.

### C. Dissociation mechanisms

The hydrogen transfer reaction (R2) leading to $SiH_4 + SiH_2$ products is found to occur in a concerted process. Figure 12 shows the time variation of the critical interatomic distances in a typical reaction at a total energy of 6.81 eV. The distance notation is as defined in Fig. 1. Up to 800 integration steps (i.s.) (1 step $= 2.038 \times 10^{-16}$ s), the Si–Si bond vibrates with a frequency less than its normal-mode frequency of 403 $cm^{-1}$ (0.002 461 i.s.$^{-1}$). At this point, Si–Si bond rupture begins to occur. Around 1200 i.s., the Si–H bond involving the hydrogen atom denoted as 3 in Fig. 1 breaks and the hydrogen atom is transferred directly to the

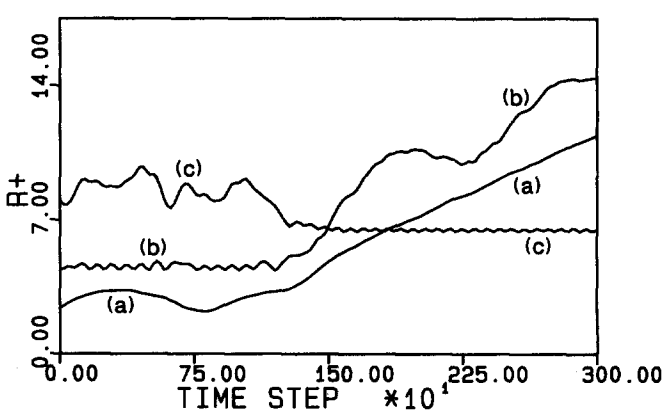


FIG. 12. Time variation of the interatomic distances in angstroms for a trajectory leading to reaction (R2) with internal energy 6.81 eV: curve (a) $R + = R_1$; curve (b) $R + = R_2 + 3.0$; curve (c) $R + = R_{11} + 5.0$. Distances are as defined in Fig. 1. One time step $= 2.038 \times 10^{-16}$ s.

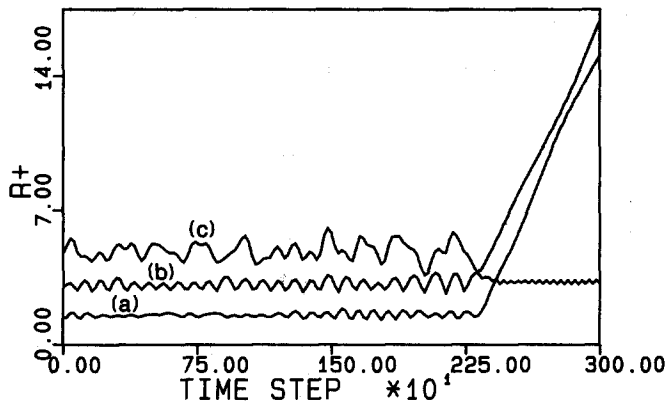


FIG. 13. Time variation of the interatomic distances in angstroms for a trajectory leading to reaction (R4) with internal energy 6.81 eV: curve (a) $R+ = R_2$; curve (b) $R+ = R_3 + 1.5$; curve (c) $R+ = R_{14} + 2.5$. Distances are as defined in Fig. 1. One time step $= 2.038 \times 10^{-16}$ s.

other silicon atom. The directness of this transfer is clearly shown by the variation of the Si(2)–H(3) distance $R_{11}$. Within 100 i.s. subsequent to the rupture of the Si(1)–H(3) bond, $R_{11}$ has decreased to the distance characteristic of a Si–H bond. It then oscillates about this distance with a frequency characteristic of a Si–H stretching mode.

Three-center $H_2$ elimination is found to be a concerted reaction in which both Si–H bonds break simultaneously followed immediately by formation of the $H_2$ bond. A typical trajectory at 6.81 eV internal energy is shown in Fig. 13. The simultaneous detachment of two hydrogen atoms (atoms 3 and 4 of Fig. 1) from Si(1) around 2400 i.s. is obvious. The immediate formation of the H–H bond is shown by the variation of $R_{14}$.

In contrast to three-center elimination, the four-center process (R6) involves the rupture of one Si–H bond followed by a transfer of this hydrogen atom to one bonded to the other silicon atom. $H_2$ formation then occurs by a mechanism that resembles a hydrogen-atom abstraction process. Figure 14 shows a typical trajectory resulting in four-center $H_2$ elimination at 6.81 eV. In this trajectory, the Si(1)–H(3) bond is seen to break around 600 i.s. H(3) then moves into the vicinity of H(7) on Si(2). This is shown by the simultaneous increase of $R_2$ and decrease of $R_{21}$, the H(3)–H(7) distance. At 850 i.s., the Si(2)–H(7) ruptures and, very soon thereafter, the H(3)–H(7) bond is seen to form.

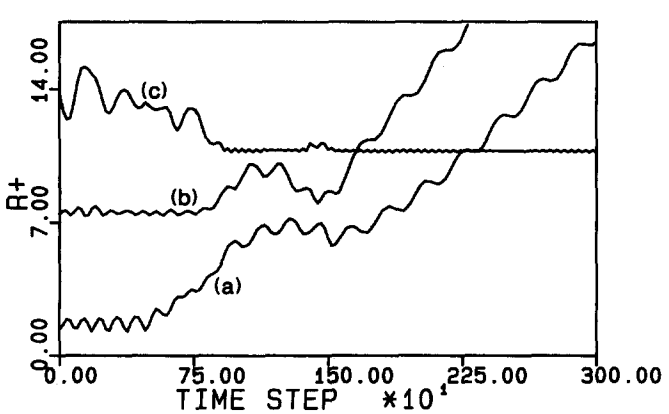


FIG. 14. Time variation of the interatomic distances in angstroms for a trajectory leading to reaction (R6) with internal energy 6.81 eV: curve (a) $R+ = R_2$; curve (b) $R+ = R_6 + 6.0$; curve (c) $R+ = R_{21} + 10.0$. Distances are as defined in Fig. 1. One time step $= 2.038 \times 10^{-16}$ s.

## ACKNOWLEDGMENTS

We are pleased to acknowledge financial support from the Air Force Office of Scientific Research under Grant AFOSR-89-0085. PMA expresses his thanks to Vikram University, Ujjain, India for granting him leave to pursue this research.

[1]For reviews, see (a) J. Bloem and L. J. Giling, *Current Topics in Materials Science*, edited by E. Kaldis (North-Holland, Amsterdam, 1978), Vol. 1, Chap. 4; (b) J. M. Jasinski, B. S. Meyerson, and B. A. Scott, Annu. Rev. Phys. Chem. **38**, 109 (1987).
[2]M. E. Coltrin, R. J. Kee, and J. A. Miller, J. Electrochem. Soc. **133**, 1206 (1986).
[3]P. M. Agrawal, D. L. Thompson, and L. M. Raff, Surf. Sci. **195**, 283(1988); J. Chem. Phys. **91**, 5021 (1989), and references therein.
[4]P. M. Agrawal, D. L. Thompson, and L. M. Raff, J. Chem. Phys. **88**, 5948 (1988) and references therein.
[5]P. M. Agrawal, D. L. Thompson, and L. M. Raff, J. Chem. Phys. **89**, 741 (1988).
[6](a) M. E. Coltrin, R. J. Kee, and J. A. Miller, J. Electrochem. Soc. **131**, 425 (1984); (b) W. G. Breiland, M. E. Coltrin, and P. Ho, J. Appl. Phys. **59**, 3267 (1986).
[7]P. Ho and W. G. Breiland, Appl. Phys. Lett. **44**, 51 (1984).
[8]D. L. Martin, D. L. Thompson, and L. M. Raff, J. Chem. Phys. **84**, 4426 (1986).
[9]D. L. Martin, D. L. Thompson, and L. M. Raff, J. Chem. Phys. (submitted).
[10](a) S. Farantos, E. C. Leisegang, J. N. Murrell, K. Sorbie, J. J. C. Texeria-Dias, and J. C. Varandas, Mol. Phys. **34**, 947 (1977); (b) S. Carter, I. M. Mills, J. N. Murrell, and A. J. C. Varandas, *ibid.* **45**, 1053 (1982).
[11]H. Gai, D. L. Thompson, and L. M. Raff, J. Chem. Phys. **88**, 156 (1988).
[12]D. L. Thompson and L. M. Raff (unpublished).
[13]L. M. Raff, J. Phys. Chem. **91**, 3266 (1987).
[14](a) J. H. Purnell, J. Chem. Soc. Faraday Trans. **69**, 1455 (1973); (b) M. Bowrey and J. H. Purnell, J. Am. Chem. Soc. **92**, 2594 (1970); (c) Proc. R. Soc. London Ser. A **321**, 341 (1971).
[15](a) E. M. Tebben and M. A. Ring, Inorg. Chem. **8**, 1787 (1969); (b) J. Dzarnoski, S. F. Rickborn, H. E. O'Neal, and M. A. Ring, Organometallics **1**, 1217 (1982); (c) R. T. White, R. L. Espino-Rios, D. S. Rogers, M. A. Ring, and H. E. O'Neal, Int. J. Chem. Kinet. **17**, 1029 (1985).
[16]G. Olbrich, P. Potzinger, B. Reimann, and R. Walsh, Organometallics **3**, 1267 (1984).
[17]M. S. Gordon, T. N. Truong, and E. K. Bonderson, J. Am. Chem. Soc. **108**, 1421 (1986).
[18]P. Ho, M. E. Coltrin, J. S. Binkley, and C. F. Melius, J. Phys. Chem. **89**, 4647 (1985).
[19]P. Ho, M. E. Coltrin, J. S. Binkley, and C. F. Melius, J. Phys. Chem. **90**, 3399 (1986).
[20]L. M. Raff and D. L. Thompson, in *Theory of Chemical Reaction Dynamics*, edited by M. Baer (CRC, Boca Raton, Florida, 1985), Vol. 3, p. 1.
[21]L. M. Raff, J. Chem. Phys. **89**, 5680 (1988).
[22]L. M. Raff, J. Chem. Phys. **90**, 6313 (1989).
[23]J. B. Pedley and B. S. Iseard, CATCH Tables, University of Sussex, 1972, 1976. Available from NTIS, Number AD-773-468.
[24]S. R. Gunn and L. G. Green, J. Phys. Chem. **65**, 779 (1961).
[25]A. M. Doncaster and R. Walsh, Int. J. Chem. Kinet. **13**, 503 (1981); J. Chem. Soc. Chem. Commun. **1979**, 904.
[26]P. Potzinger and F. W. Lampe, J. Phys. Chem. **74**, 719 (1970).
[27]T. N. Bell, K. A. Perkins, and P. G. Perkins, J. Chem. Soc. Faraday Trans. **77**, 1779 (1981).
[28]J. Berkowitz, J. P. Greene, and H. Cho, J. Chem. Phys. **86**, 1235 (1987).
[29]JANAF Thermochemical Tables, Dow Chemical Company, distributed by Clearinghouse for Federal Scientifc and Technical Information, PB168370 (1965) and subsequent updates.
[30]A. J. Vandsewielen, M. A. Ring, and H. E. O'Neal, J. Am. Chem. Soc. **97**, 993 (1975).